Numerical and experimental investigation of inlet velocity influence on airflow characteristics for indoor thermal comfort

Hasna Abid [1, 2], Ridha Djebali [3, *], Hamza Faraji [4], Mariem Lajnef [1], Zied Driss [1], Jamel Bessrour [3]

[1]Laboratory of Electro-Mechanic Systems (LASEM), National School of Engineers of Sfax (ENIS), University of Sfax, B.P. 1173, km 3.5 Road Soukra, 3038 Sfax, Tunisia

[2]National School of Engineers of Tunis (ENIT), University of Tunis Manar, BP 37, le Belvedere, 1002 Tunis, Tunisia

[3]UR22ES12: Modeling, Optimization and Augmented Engineering, ISLAI Béja, University of Jendouba, Béja 9000, Tunisia

[4] LISA Laboratory, National School of Applied Sciences, Cadi Ayyad University, Marrakech, Morocco

* Corresponding author:
Pr. Ridha Djebali
Email: ridha.djebali@islaib.u-jendouba.tn

Abstract

In recent decades, researchers have focused on indoor thermal comfort due to its significant impact on human health and work productivity. Various factors affect airflow characteristics and thermal comfort in indoor environments. This study thoroughly investigates the impact of input velocity on indoor airflow and thermal comfort. A numerical model was developed, complemented by an experimental setup, and validated through a detailed comparison with test data—specifically, air velocity and data from a cabin test occupied by a human body. To ensure simulation accuracy, turbulence and grid independence analyses were consistently incorporated into the numerical model optimization. Numerous simulations examined the effects of inlet velocity. The analysis shows that airflow characteristics within the cabin test are mainly influenced by input velocity. Moreover, a comparative analysis demonstrates a direct impact of input velocity on the thermal comfort index. The maximum expected PD% value for $V=1\ m.s^{-1}$ increases significantly, by 1.6, 2.2, and 2.63 times, respectively, compared to values at $V=0.5\ m.s^{-1}$, $V=0.33\ m.s^{-1}$, and $V=0.25\ m.s^{-1}$. In summary, this study highlights the substantial influence of inlet velocity on indoor airflow and thermal comfort, underscoring the importance of precise modeling and control for creating an optimal indoor environment.

Keywords:
Inlet velocity, indoor airflow characteristics, thermal comfort, numerical model, experimental setup,

1. Introduction

Nowadays, ensuring thermal comfort is of utmost importance for occupants in indoor environments [1] (Zhang, Cheng, Fang, Huan, Lin,2017). For occupant well-being and workplace productivity, maintaining adequate air quality and ensuring thermal comfort in indoor environments is crucial [2] (Akimoto, Tanabe, Yanai, Sasaki, 2010). To satisfy the thermal requirements in indoor areas Heating Ventilation and Air Conditioning (HVAC) procedures are required [3] (Shi, Lu, Chen, 2019). Studies have been done to identify the factors, such as the effect of room geometry, that can influence indoor thermal comfort. The impact of the location and quantity of openings has been the subject of several research. For instance, Li et al. [4] affirmed that the outlet position had less of an influence than the placement of the inlet aperture. Using a validated CFD model, Motlagh et al. [5] studied the importance of maintaining indoor air quality in Operating Rooms (ORs) to mitigate infection risks during surgeries. The study compares the impact of Turbulent and Laminar Airflow (TAF/LAF) systems on air and CO2 distribution, concluding that LAF systems, particularly with an air curtain configuration, significantly reduce CO2 concentration levels in the OR, enhancing patient and surgical team safety. Shetabivash [6] examined the effects of the location and form of the aperture on natural ventilation. The performance of the airflow pattern in indoor spaces is discovered to be influenced by the size and placement of the opening. Qin et al. [7] focuses on optimizing ventilation in densely occupied spaces like classrooms during the COVID-19 pandemic. Using an impinging jet ventilation system, the research emphasizes that strategically placing exhausts, especially near regions with high contaminant concentration, is crucial for effective contaminant removal. they found that a single exhaust, located on the same side as the supply diffuser, outperforms evenly distributed exhausts, significantly improving indoor air quality in terms of mean age of air, CO2 concentration, and tracer gas concentration.

The location of the intake and outlet openings in the ventilation strategy under consideration has a direct impact on the indoor airflow, according to research by Karava et al. [8] on the influence of opening position on cross-ventilation. Mohammed [9] used numerical calculations and actual measurements to forecast indoor airflow using various diffuser forms, including square and circular ceiling diffusers. To determine the boundary conditions at the swirl diffuser's inlet simply, Zhou et al. [10] split a circular diffuser into six triangular sectors with identical air discharge rates. To assess the impact of boundary conditions on indoor settings, a detailed bibliographic search was done. Stamou et al. [11] introduced a varied intake temperature to the Galatsi Arena stadium to assess thermal comfort and discovered that an incoming temperature of 16°C offered thermal satisfaction. Abid and Driss [12] investigate the surface of inlet holes impact on the airflow characteristics and thermal comfort in an enclosed space occupied by a thermal manikin, through a combination of computational studies and experimental validation. To investigate the effect of airflow velocity on thermal conditions in a heated room, Kobayashi et al. [13] carried out numerical research where the total supply airflow rate into the room was constant. The vertical temperature profile was found to be directly affected by the supply air velocity, as revealed by the analysis. Additionally, Chen et al. [14] used the validated model to examine the effects of various flow and configuration factors on the impinging jet flow field, including diffuser shape and supply airflow rate. Sheng et al. [15] examines a novel all-air wall induction unit designed for hospital ward use, focusing on its ventilation and thermal performance. In fact, they measure and analyze steady-state temperature and CO2 concentration distributions under various supply conditions. Mohammed [16] also examined the effect of input temperature and velocity on the indoor environment by numerical modeling. He discovered that a comfortable indoor environment may be created even with a modest input velocity. Wang et al. [17] explores the effectiveness of cross-shaped columns in ventilation, comparing them with conventional square and circular column attachment ventilation models. Numerical simulations and experiments were conducted to analyze air distribution in isothermal conditions and the thermal environment under cooling conditions. they found that the cross-shaped column showed distinct airflow patterns and increased kinetic energy loss at the column bottom compared to square columns. When Noh et al. [18] examined the impact of different airflow on ventilation efficiency, they discovered that raising the air change rate resulted in better air quality. The impact of occupant and heat source intensity on the indoor environment and air quality has also been extensively studied in the literature. With three thermal conditioning systems radiators, underfloor heating, and radiant ceiling and altering their placement in the indoor space. Rabanillo-Herrero et al. [19] examined the efficiency of air change. They discovered a clear relationship between a room's airflow and ventilation efficiency and the location of the heating source. The direct relationship between the position of the heat source and ventilation rate was shown by Tlili et al. [20]. Anthony et al. [21] compared the performance of two models, the elliptic blending differential flux model (EBDFM) and the standard differential flux model (DFM), in simulating turbulent natural convection in a square cavity. The study modifies a model coefficient to promote turbulence in the boundary layer, improving the accuracy of computed mean quantities compared to experimental data. While both models have some discrepancies, the EBDFM generally performs better, particularly in predicting turbulent quantities, indicating the advantage of its approach in near-wall turbulence modeling. Thermal comfort evaluation must be considered in these various circumstances. Ganesh et al. [22] presented a literature review on Indoor Environment Quality (IEQ) focusing on thermal comfort. It discusses the complexity of thermal comfort, the classification of literature based on methodologies and comfort parameters, factors affecting IEQ and thermal comfort, evaluation methods, and related issues like sick building syndrome. The review emphasizes the importance of IEQ and factors affecting human thermal comfort, aiming to simplify the relationship between comfort parameters, occupant well-being, and IEQ for designers, engineers, and researchers. ISO 7730 evaluates the Fanger-developed PMV (Predicted Mean Vote) and PPD (The Predicted Percentage of Dissatisfied) thermal sensation scales. Vithanage et al. [23] assesses thermal comfort in the Mechanical Lecture Room (MLR) at the University of Ruhuna. Using two 36000Btu/h Split Type air conditioners, the researchers varied room temperature from 18.5 to 24.6 C°. The study, conducted in a room with dimensions 14.66m x 5.10m x 5.13m, employed 10 thermocouples to collect temperature data. Ahmed et al. [24] observed that thermal comfort increased when exhaust outlets were combined in the presence of certain heat sources within the room, such as the ceiling, while estimating the effect of exhaust diffuser position on thermal comfort in an inhabited office area. Using the PMV and PPD indices, Abid et al. [25] examined the impact of entrance velocity on indoor thermal comfort and discovered that an increase in input velocity may result in a chilly sensation. In addition, the proportion of respondents who were dissatisfied with the draft (PD) was employed in the bibliographies research (Fanger et al. [26]) for draft assessments. According to Ahmed et al. [27] investigation of the effect of local exhaust height on thermal comfort inside, all treated instances had PD values that were comfortably within the desired range. Abid et al. [28] investigated the impact of Reynolds number on the thermal comfort index of PD% using simulated techniques with precise data. Ganesh et al. [29] evaluates the impact of different inlet and exhaust vent profiles on indoor occupant comfort and energy efficiency in cold climate conditions. The research analyzes various ventilation configurations based on comfort parameters such as PMV, PPD, air temperature, temperature gradient, and fluid flow velocity. The findings highlight the significant effect of ventilation profiles on both IEQ and energy consumption, emphasizing the importance of selecting optimized ventilation strategies for sustainable buildings in cold climates. The literature research indicates that the indoor atmosphere is significantly influenced by building design. However, there is still a sizable knowledge gap regarding the correlation equations between the indoor airflow features that have not been considered and the boundary conditions at the entrance. As a result, the major goal of this study is to ascertain how intake velocity, while keeping the supply airflow rate constant, affects the airflow characteristics and the level of comfort within a ventilated cabin prototype that is occupied by a thermal manikin. Therefore, a numerical simulation and experimental research were carried out. ANSYS Fluent 17.0 was used to carry out the numerical simulations. The structure of this article is as follows: A overview of the literature on the many factors influencing the indoor environment and thermal comfort is presented in Section 1. The test cabin and the experimental procedure's approach are presented in Section 2. The physical layout of the test cabin that contains a human body and the choice of numerical parameters are provided in Section 3. For various input velocities, Section 4 shows the numerical findings for the velocity fields, the temperature, the static pressure, the turbulent kinetic energy, and the turbulent viscosity within the test cabin. Moreover, correlation equations were developed to establish the relationship between the inlet velocity and the maximum values of temperature, static pressure, and turbulent features. The following section includes information on how intake velocity affects indoor thermal comfort. The main conclusions of this study are presented in Section 6, which closes this essay.

2. Experimental procedure

An experimental investigation was conducted to validate the accuracy of the Computational Fluid Dynamics (CFD) simulation and ensure the reproducibility of the employed methodology. This study was carried out at National School of Engineering of Sfax, University of Sfax, Tunisia, in North Africa (34.7271° N, 10.7193° E). The dimensions of the test cabin, depicted in Figure 1 and table 1, are 1.88 m in length, 1 m in width, and 1.45 m in height. The cabin incorporates two circular apertures, each with a diameter of 0.1 m, positioned at the y=0.5 m plane within the cabin. The walls of the cabin possess a thermal conductivity of λ=0.061

$W.m^{-1}. K^{-1}$. To simulate an indoor heat load, a thermal manikin shaped like a standing human body was centrally placed within the cabin and covered with aluminum sheets, as indicated in figure 1.c. The experiment entails the use of a wire string encircling the manikin to induce heat through conduction. This wire, acting as an electrical resistance, generates a thermal power. By applying an electric current to the wire, it transforms into a heat source, thereby warming the thermal manikin and releasing heat into the cabin. These electric heaters, producing 45 $W.m^{-2}$ of heat, envelop the human body, equivalent to the average sensible heat generated by a standing person. This methodology enables the simulation of thermal conditions in a human-occupied environment, facilitating the analysis of thermal interactions within the cabin. After one hour and a half the steady-state condition was achieved, measurements were taken at various locations throughout the cabin. These measurements encompassed velocity and temperature data and were used to establish boundary conditions for numerical simulations. DHT22 sensors, featured in Figure 1.c, were strategically positioned to monitor air temperature. These sensors exhibit a resolution of 0.1°C, an accuracy of ±0.5°C, and a wide measuring range from -40°C to +80°C, ensuring comprehensive coverage across designated areas. Velocity within the cabin volume was measured using hot-wire anemometers of type AM 4204 at various locations presented in figure 1.d. In addition table 2 presents the Hot-wire anemometer type AM 4204 characteristics. The accuracy of the numerical simulations was subsequently verified by comparing them against these experimental measurements, ensuring a robust validation of the CFD model.

3. Numerical model

The process of numerical modelling and validating test cabin simulations using ANSYS 17.0 encompasses three essential stages: pre-processing, solving, and post-processing (Rajabpour et al.[30]). During the pre-processing stage, the primary focus lies in developing the test cabin's geometry within ANSYS Design Modeler and creating a mesh using the ANSYS Meshing Application. This entails accurately representing the physical characteristics of the test cabin, including its dimensions, the precise position and geometry of the human body, and the locations of ventilation systems. Once the geometry is constructed, it undergoes meshing to generate a computational grid consisting of cells that span the entire volume of the test cabin.

The solving stage involves configuring the materials and boundary conditions, selecting models, and specifying solution parameters for the numerical simulation. Materials are assigned to different parts of the test cabin, such as modelling the indoor air as Boussinesq air. Boundary conditions are established based on the characteristics of the ventilation systems, convection heat from the human body and the adiabatic walls. The simulation employs models based on fluid dynamics equations, including the 3D Reynolds-Averaged Navier-Stokes (RANS) equations. Solution parameters are carefully chosen to ensure accuracy and efficiency in the simulation.

In the post-processing stage, the numerical results are presented and analysed within ANSYS Fluent and CFD-Post. Once the simulation is completed, the results are interpreted through graphical representations. Various parameters such as velocities, temperature, static pressure, turbulent kinetic energy, and turbulent viscosity are evaluated at different locations within the test cabin.

The validation of the test cabin simulation is a crucial step in assessing the reliability of the numerical model. This involves comparing the numerical results with experimental data obtained from physical measurements conducted within the test cabin. In the case of the test cabin simulation, experiments were performed in a setup equipped with mechanical ventilation, utilizing sensors like AM 4204 Hot-wire anemometers to measure air velocity and air temperature. The simulation results were then compared to the experimental data to validate the accuracy of the numerical model.

3.1. Governing equations

The focus of this section is on the governing equations utilized in this study to model turbulent incompressible flow, which include the steady-state Reynolds-averaged Navier-Stokes (RANS) equations for the conservation of mass and momentum (ANSYS [31]- Abid et al. [32]).

The continuity equation is written as follows (Norouzi et al. [33]- Chiboub et al. [34]):

$$\frac{\partial}{\partial x_i}(\rho u_i) = 0 \tag{1}$$

The momentum equation are written as follows (Jo et al.[35]):

$$\frac{\partial}{\partial x_j}(\rho u_i u_j) = -\frac{\partial p}{\partial x_i} + \frac{\partial}{\partial x_j}\left[\mu\left(\frac{\partial u_i}{\partial x_j} + \frac{\partial u_j}{\partial x_i}\right)\right] + \frac{\partial}{\partial x_j}(-\rho\,\overline{u_i' u_j'}) \tag{2}$$

Where ρ presents the density (kg.m^{-3}), p presents the pressure (Pa), μ presents the dynamic molecular viscosity (kg.m^{-1}.s^{-1}), x_i presents the cartesian coordinate (m) for i=1, 2, 3, u_i presents the velocity component in the x_i direction (m.s^{-1}), δ_{ij} presents the Kronecker delta and $\rho\,\overline{u_i' u_j'}$ presents the Reynolds stresses.

The approach adopted follows the Boussinesq hypothesis connecting the Reynolds stresses with mean velocity gradients (Zhang et al. [36] and Foroozesh et al. [37])

$$-\rho\,\overline{u_i' u_j'} = \mu_t\left(\frac{\partial \mu_i}{\partial x_j} + \frac{\partial \mu_j}{\partial x_i}\right) - \frac{2}{3}\rho k \delta_{ij} \tag{3}$$

In equation (3), μ_t presents the turbulent viscosity (kg.m^{-1}.s^{-1}) and k presents the turbulent kinetic energy (m^2.s^{-2}).

$$k = \frac{1}{2}\overline{u_i' u_j'} \tag{4}$$

The following format can be used to express the energy equation:

$$\frac{\partial T}{\partial t} + u_j \frac{\partial T}{\partial x_j} = \frac{\partial}{\partial x_j}\left[a \frac{\partial T}{\partial x_j}\right] \tag{5}$$

where $a = \frac{\lambda}{\rho c_p}$ is the fluid thermal diffusity (m^2.s^{-1}).

The turbulence viscosity for the k-ε turbulence model is given by:

$$\mu_t = \rho C_\mu \frac{k^2}{\varepsilon} \tag{6}$$

where C_μ is a constant and ε is the dissipation rate.

The turbulence viscosity for the k- ω turbulence model is calculated by

$$\mu_t = \rho_f \frac{k}{\omega} \quad (7)$$

where ω is turbulent frequency.

3.2. CFD modelling

Figure 2 illustrates the computational domain, acquired through Design Modeler, for configuring the experimental setup. Simultaneously, Table 1 provides a comprehensive overview of the geometric characteristics of the cabin. The geometry of the test cabin features two circular openings with a diameter (D) of 0.1 m, strategically positioned at the median plane (y=0.5 m). The first opening, situated at a height (h_1) of 0.095 m from the floor, facilitates the inflow of outside air into the cabin. In contrast, the second opening, positioned at a height (h_2) of 1.2 m from the first opening, serves as an outlet for airflow from the cabin. The cabin walls are assumed to be adiabatic, adhering to no-slip conditions. The thermal manikin within the cabin is modelled based on its actual dimensions, including a height of 1 m, a surface area of 0.74 m^2, and a convective heat output of 34 W. Various boundary conditions, depicted in Fig. 3 and detailed in Table 3, were applied to simulate the experimental scenario accurately.

3.3. Meshing selection

Ensuring the accuracy of a CFD numerical simulation begins with the judicious selection of an appropriate mesh. In our study, we employed the ANSYS meshing tool to generate a tetrahedral unstructured grid, tailored to the intricate design of the prototype. To capture the aerodynamic intricacies surrounding the thermal manikin, we incorporated ten fine layers around the manikin itself, as well as in proximity to the inlet and outlet openings. In this section of our investigation, we developed four distinctive grids, each characterized by varying node counts (162 589, 237 030, 323 270, and 486 599). These diverse grid configurations played a pivotal role in conducting a thorough assessment of result reliability, as illustrated in Figure 3 and systematically detailed in Table 4. Figure 4 visually showcases the mesh structure for the grid comprising 323,270 nodes. Notably, the velocity values at a specific location denoted by coordinates x=0.74 m, y=0.5 m, and z=0.05 m are depicted in Figure 5 for the different meshes. It is noteworthy that meshes 3 and 4 exhibit commendable alignment with experimental results, as evidenced by the visual comparison presented in this figure. As the resolution time grows along with the node count (Nazemian et al. [38]). Therefore, the 323270 nodes mesh was selected to balance accuracy and computational efficiency.

3.4. Turbulence modeling choice

The selection of an appropriate turbulence model is pivotal, contingent upon a meticulous comparison between experimental data and numerical simulation findings. In our study, we systematically evaluated various turbulence models against experimental temperature data, specifically focusing on directions denoted by (a) x = 0.2 m and y = 0.5 m, and (b) x = 0.74 m and y = 0.5 m, as illustrated in Figure 6. This comprehensive analysis distinctly underscores the substantial impact of the turbulence model on the temperature distribution. Evidently, the SST k-ϖ model emerged as the most fitting turbulence model for our numerical simulations, designed to probe the behavior of interior environments. The determination of the SST k-ϖ model as the optimal choice was informed by the outcomes of the CFD analysis, revealing the highest level of agreement with the experimental data. This judicious selection emphasizes the critical role played by an appropriate turbulence model in ensuring the accuracy and reliability of numerical simulations, particularly in the nuanced study of the thermal behavior within interior environments. Table 5 depicts the standard error between the experimental temperature data and the corresponding values predicted by the numerical model. The standard error quantifies the average difference between these two sets of values. The specific formula used to calculate the standard error is provided in (Abid et al. [39]-Hannachi et al. [40]):

$$Sd = \frac{(N - Exp)}{Exp} \times 100 \tag{8}$$

In this formula, 'N' represents the temperature predicted by the numerical model and 'Exp' represents the experimentally measured temperature, specifically at the location defined by x=0.2 m and y=0.5 m on the visualization plane. The close agreement between the experimental data and the numerical predictions suggests good alignment with the SST k-ω turbulence model. Moreover, the adoption of the SST k-ω turbulence model is consistent with a widely accepted practice in indoor environment modeling, as substantiated by prior research conducted by Abid et al. [41]. Recognized for its efficacy in capturing turbulence effects within confined spaces, the SST k-ω model has gained prominence within the scientific community. This decision to employ the SST k- ω turbulence model is therefore rooted in established precedent, fortifying the credibility of our simulation approach and reinforcing its alignment with established methodologies in the field of indoor environment studies.

3.5. Computational schemes and settings

To evaluate the airflow dynamics and heat transfer within the cabin test occupied by Thermal Human body, we conducted a simulation of an incompressible, low-speed flow using a pressure-based solver. Employing a second-order upwind strategy, default sub-relaxation variables for pressure, density, momentum, and k- ω were utilized. The convergence acceleration was achieved through the implementation of the SIMPLEC solver algorithm. Post-processing was carried out using Ansys Fluent 17.0 to visualize and analyze the numerical data generated. To understand the influence of inlet velocity on airflow characteristics and indoor thermal comfort, a series of simulations were conducted.

4. Airflow characteristics

This section investigates how indoor airflow characteristics and thermal comfort are impacted by input supply velocity. Four alternative situations were taken into consideration while keeping the same supply airflow rate of Q=0.0078 $m^3.s^{-1}$ to evaluate this influence. Figure 7 depicts the computational domain for each scenario, whereby one, two, three, and four inlet apertures were offered. For each scenario, inlet velocities of V=1 $m.s^{-1}$, V=0.5 $m.s^{-1}$, V=0.33 $m.s^{-1}$, and V=0.25 $m.s^{-1}$ were used, while an inlet temperature of T=301 K was kept constant as presented in table 6. The goal was to determine how the various input velocities affected the distribution of the velocity fields, temperature, static pressure, turbulent kinetic energy, and turbulent viscosity inside the test cabin.

4.1. Validation of the developed model

For varying inlet velocities of V=1 $m.s^{-1}$, V=0.5 $m.s^{-1}$, V=0.33 $m.s^{-1}$, and V=0.25 $m.s^{-1}$, where one, two, three, and four inlet apertures are given, respectively, Figure 8 shows the evolution of velocity profiles in the plane defined by y=0.5 m. The test cabin's x=0.2 m and x=0.72 m was used to designate the directions in which the profiles were taken. These profiles make it obvious that the velocity appears to be identical. The direction described by x=0.2 m and x=0.72 m, which is closest to the intake opening, is where the two planes connect, and this is where the greatest velocity value is found. As a result, the velocity profiles are significantly influenced by the input velocity and the quantity of supply apertures. Additionally, the profiles demonstrate that, with a variance of around 7%, the numerical results for V=1 $m.s^{-1}$ are in good agreement with the experimental data. These outcomes attest to the precision of the numerical approach.

4.2. Velocity fields

The results of the CFD simulations performed for various input velocities show that the supply velocity has a significant impact on the velocity distribution inside the test cabin. The discharge zone at the intake aperture that invades the human body is depicted by the velocity fields in the plane specified by y=0.5 m, as seen in Figure 9. This emphasizes how crucial it is to position the intake apertures correctly to provide thermal comfort and prevent direct contact between the people inside and the incoming air. Above the thermal mannequin, the presence of a thermal plume caused by buoyancy is evident. This thermal plume is influenced by the inlet velocity. As the flow flows further away from the thermal plume, the velocity values progressively decrease, demonstrating a well-mixed air dispersion. In all instances, the existence of recirculation zones indicates that the cabin is successfully combining the room air with the supply air. These results are promising, as good air mixing is crucial for maintaining a uniform temperature and providing thermal comfort to the occupants. The velocity profiles in the cross-plane denoted by y=0.5 m for various supply velocities is also shown in Figure 10, which sheds light on the velocity dispersion downstream of the thermal manikin. These profiles show that the intake opening's existence causes the air velocity to constantly be in an acceleration zone. The velocity values drop as the flow gets nearer to the thermal manikin, showing that the manikin is successfully heating the surrounding air. To attain the appropriate degree of thermal comfort, the position and quantity of intake ports may be optimized using this information, which is crucial for comprehending the thermal behavior inside the test cabin.

4.3. Temperature

When examining the temperature distribution in the test cabin, the findings demonstrate the critical role of inlet velocity in shaping the overall temperature distribution. As illustrated in Figure 11, varying the inlet velocity from V=1 $m.s^{-1}$ to V=0.25 $m.s^{-1}$, along with an increase in the number of inlet openings, reveals a clear thermal stratification. The highest temperature, T=307 K, is observed above the human body's head. This phenomenon is crucial in fluid dynamics, particularly in understanding natural convection, where fluid motion is primarily driven by buoyancy forces. Changes in velocity affect the flow pattern and temperature distribution within the fluid. In the context of natural convection, increasing velocity enhances fluid mixing, leading to a more uniform temperature distribution. The temperature at the inlet opening, T=301 K, was observed to be influenced by the boundary conditions. Furthermore, at an inlet velocity of V=1 $m.s\text{-}^{1}$, the heat manikin's temperature is slightly higher on the right side due to the presence of only one inlet opening.

The temperature profiles in Figure 12, which compare the different situations along the directions specified by x=0.2 m and x=0.72 m, reveal that although minor temperature variations exist, the profiles appear to be similar. The air temperature value in the top section of the cabin is also affected by the incoming air velocity, with the temperature being lowest when the inlet velocity is V=1 $m.s^{-1}$. Based on the CFD results, Equation 9 provides a correlation equation between the inflow velocity V and the maximum temperature value, with a determination coefficient of R^2=0.98. These results provide valuable insights into how the temperature distribution in the test cabin is influenced by the inlet velocity and the number of inlet openings.

$$T_{max} = -1.2\,V^2 - 1.36\,V + 324.11 \tag{9}$$

4.4. Static pressure

The numerical simulation performed on the test cabin with different inlet velocities, such as V=1 $m.s^{-1}$, V=0.5 $m.s^{-1}$, V=0.33 $m.s^{-1}$, and V=0.25 $m.s^{-1}$, sheds light on the critical role of static pressure distribution in regulating the indoor air quality and thermal comfort as well as controlling the airflow resistance. The static pressure distribution in the plane indicated by y=0.5 m shows a compression zone near the test cabin's intake, followed by a reduction in static pressure in the discharge zone, as shown in Figure 13. With a depression zone at the outflow aperture, the static pressure is nearly constant throughout the test cabin. The results comparison shows how intake velocity directly affects static pressure distribution. To establish a correlation between the inlet velocity and the maximum static pressure value, equation 10 was derived from the CFD results. It is crucial to note that equation 10 has a determination coefficient of R^2=0.98, indicating a high degree of accuracy in predicting the maximum static pressure value. Hence, proper control of static pressure is necessary to ensure good indoor air quality and thermal comfort.

$$p_{max} = 0.27\,V^2 - 0.11\,V + 0.99 \tag{10}$$

4.5. Turbulent kinetic energy

A crucial factor in assessing indoor air quality and thermal comfort is the distribution of turbulent kinetic energy in the plane indicated by y=0.5 m, which is shown in Figure 14. Heat transmission, indoor pollutant dispersion, and air distribution patterns are all significantly influenced by turbulent kinetic energy. As the air flows through the cabin, the data show that the turbulent kinetic energy steadily declines after reaching its peak at the intake entrance. It's interesting to note that there isn't much kinetic energy in the turbulent flow surrounding the human body and the outlet opening. The direct influence of the input velocity on the turbulent kinetic energy distribution is highlighted by comparing the numerical results. Then, it proposed Equation 11 to correlate the input velocity V with the maximum turbulent kinetic energy, as obtained from CFD simulations. The equation provides a good fit to the data, as evidenced by the high determination coefficient R^2=0.98.

$$k_{max} = 0.144\,V^2 - 0.01\,V + 0.0034 \tag{11}$$

4.6. Turbulent Viscosity

Figure 15 displays the distribution of turbulent viscosity at various input velocities in the plane defined by y=0.5 m. In indoor conditions, the parameters of airflow and heat transport are significantly influenced by turbulent viscosity. Variations and vortices that create eddies and transport mass, momentum, and heat are characteristics of turbulent flows [31]. Therefore, a precise model of turbulent viscosity is crucial for predicting airflow patterns, temperature distributions, and indoor air quality. The results show that as the airflow flows through the cabin, the turbulent viscosity steadily decreases, peaking at the entrance aperture. The reason why the turbulent viscosity is greatest in front of the human body may be due to the room's recirculation zone. The numerical findings are also contrasted to show that the entrance velocity has a direct impact on the distribution of turbulent viscosity. To summarize, maintaining high indoor air quality and thermal comfort requires a knowledge of the distribution of turbulent viscosity. Equation (13), which may be used to estimate the relationship between the input velocity V and the maximum turbulent viscosity, provides important information for building effective ventilation systems.

$$\mu_{max} = 0.0031\,V^2 - 0.0016\,V + 0.0022 \tag{13}$$

5. Thermal sensation assessment

5.1. Thermal sensation indicator PMV

Thermal sensation is assessed using the Predicted Mean Vote (PMV) indicator (Fanger et al. [42]). This indicator runs from -3 to +3, with values corresponding to a chilly to hot sensation, and is based on the heat transfer between the human body and its surroundings. When the PMV indicator fluctuates between -0.5 and +0.5, it is considered very comfortable, while it is considered comfortable when it ranges between -1 and +1 per ISO 7730 [43]. The PMV indicator is influenced by several variables, including the respiration rate, the body temperature, the clothing, the air velocity, and the relative humidity.

PMV = (0.303 * exp (-0.036 * M) + 0.028) * (M - W) - 3.05 * 10^(-3) * (5733 - 6.99 * M – P_a) - 0.42 * (M - W - 58.15) (14)

where:

- M is the metabolic rate of the person (expressed in watts per square meter)
- W is the external work being performed by the occupant (expressed in watts per square meter)
- P_a is the partial pressure of water vapor in the air (expressed in kilopascals)

In this study, CFD results were used to determine the air temperature and air velocity for each scenario. Additional parameters included setting relative humidity, clothing, and metabolic rate to 0.8 met, 0.5 clo, and 50%, respectively. Figure 16 shows the resultant PMV profiles for different input velocities along the x=0.2 m and x=0.72 m directions in the plane defined by y=0.5 m. In both orientations, the PMV profiles appear to be the same. However, it was found that the PMV value decreased as the number of input holes increased. When the PMV value was about 1.5 at z higher than 1 m, the maximum value of PMV was attained, signifying an agreeable degree of warmth. This number may be explained by the presence of a thermal plume, which occurs when velocity and temperature reach their maximum levels.

5.2. Thermal sensation PD indicator

The potential issue of cold drafts due to higher velocities near the floor can cause discomfort, especially for individuals who are stationary or seated in these areas. This discomfort not only affects their immediate well-being but can also lead to a decrease in productivity and overall satisfaction with the indoor environment. Additionally, prolonged exposure to these drafts can have significant health effects, particularly for vulnerable populations such as the elderly or those with respiratory conditions. Cold air drafts can exacerbate conditions like arthritis and lead to muscle stiffness, highlighting the importance of addressing this issue. Addressing cold drafts is beneficial not only for comfort and health but also for energy efficiency. When occupants feel colder due to drafts, they may increase the heat, leading to higher energy consumption. Implementing strategies to mitigate cold drafts, such as improving insulation and sealing gaps and cracks in windows, doors, and walls, can enhance comfort and health while also contributing to improved energy efficiency. To evaluate the likelihood of draughts in a building, Fanger's percentage of unhappy persons owing to draught (PD), based on the standardized thermal comfort empirical equation ISO 7730, can be used. This equation predicts the proportion of persons who would feel uncomfortable due to draught by considering factors like air temperature, air velocity, and humidity. The PD value is calculated based on the air velocity relative to the predetermined thermal comfort range. This indicator allows building designers and engineers to assess and control the risk of draughts in structures, ensuring that occupants are comfortable and safe:

$$PD = 3.413\,(34 - T_a)\,(V_a - 0.05)^{0.622} + 0.369\,V_a T_u\,(34 - T_a)\,(V_a - 0.05)^{0.622} \quad (15)$$

Where T_a, V_a and T_u are respectively the air temperature, the air velocity and the air turbulent intensity. For $V_a < 0.05$, we consider V_a=0.05 m.s^{-1} and for PD> 100%, we consider PD=100 %. Figure 1**7** in the plane specified by y=0.5 m shows the PD indicator profiles for various input velocities along the x=0.2 m and x=0.72 m directions. The PD index is a key indicator for evaluating indoor thermal comfort and quantifying the number of occupants unhappy due to draughts. The results indicate that as the number of intake openings increases, the PD indicator decreases. Moreover, the highest anticipated PD% value for V=1 m.s^{-1} increases significantly, by 1.6, 2.2, and 2.63 times compared to values attained by V=0.5 m.s^{-1}, V=0.33 m.s^{-1}, and V=0.25 m.s^{-1}, respectively. These findings suggest that under all considered conditions, thermal comfort is ensured within the test cabin. Notably, the inlet velocity directly affects the predicted percentage of dissatisfied people (PD %) and, therefore, indoor thermal comfort. These results provide valuable insights for developing ventilation systems that enhance thermal comfort and minimize draught concerns in structures.

6. Discussion and Limitations

The present study lays the groundwork for future research in indoor environment and thermal comfort control. By examining the impact of inlet velocity on indoor environments, this study offers valuable insights that can enhance the development of more precise and accurate simulation models. These models, in turn, can facilitate improved indoor environment and thermal comfort management practices, ultimately leading to optimized indoor environments. The robust correlations presented in this study can serve as a basis for the development of predictive models that enable real-time climate control in indoor environments. Overall, the study's findings point toward a promising direction for future research in indoor environments, with the potential to contribute significantly to the development of comfortable indoor climates. However, some important aspects were not fully explored in this study. For example, future research could investigate indoor environment dimensions with varying climate conditions. By considering these factors, future studies can provide a more comprehensive understanding of the indoor environment and its impact on indoor thermal comfort. Such investigations can lead to the development of more effective indoor management strategies that can further enhance indoor thermal comfort.

7. Conclusion

The impact of input velocity on airflow characteristics and thermal comfort is investigated in this study. The model's distinctive and innovative features are emphasized through a comparative analysis with previous research, making a significant contribution to the field. The study employs a comprehensive Computational Fluid Dynamics (CFD) model and implements an experimental setup to ensure accuracy. Validation of the numerical results is conducted using a human body placed within an experimental test chamber. Optimal mesh resolution is determined through grid analysis, with the SST k-ω model identified as the most suitable choice based on turbulence model selection research. Furthermore, the analysis of numerical data yields promising results, revealing minimal error in air velocity profiles and high agreement between experimental and numerical outcomes.

The validated results lead to the following conclusions:

- The recirculation zones inside the cabin prototype depend on the inlet velocity.

- The indoor cabin temperature is significantly impacted by inlet velocity. In fact, the temperature being lowest when the inlet velocity is $V=1\ m.s^{-1}$

-The intake velocity exerts a discernible impact on the static pressure maps, with $V=1\ m.s^{-1}$ yielding the highest static pressure among the considered velocities.

- It has been observed that the maximum value of turbulent kinetic energy increases with higher inlet velocities. Specifically, the maximum turbulent kinetic energy values are $k = 0.0099\ m^2.\ s^{-2}$ for $V = 0.25\ m.\ s^{-1}$ and $k = 0.1374\ m^2.\ s^{-2}$ for $V = 1\ m.\ s^{-1}$.

-The PMV value exhibits a decrease as the number of inlet holes increases, as evidenced by the outcomes of PMV thermal sensation tests.

-Thermal comfort evaluations utilizing the Predicted Percentage of Dissatisfied (PD%) indicate a direct influence of input velocity on this measure, highlighting the significance of intake velocity in assessing thermal comfort.

Funding

The author(s) received no financial support for the research, authorship, and/or publication of this article.

Conflict of interest

The author(s) declared no potential conflicts of interest with respect to the research, authorship, and/or publication of this article.

References

[1]. Zhang, S., Cheng, Y., Fang, Z. et al. “Optimization of room air temperature in stratum-ventilated rooms for both thermal comfort and energy saving.” *Applied Energy*, 204, 420–431. doi:10.1016/j.apenergy.2017.07.064 (2017).

[2]. Akimoto, T., Tanabe, S., Yanai, T et al. “Thermal comfort and productivity – Evaluation of workplace environment in a task conditioned office. “Building *and Environment*, 45(1), 45–50.(2010) doi:10.1016/j.buildenv.2009.06.022

[3]. Shi, Z., Lu, Z., Chen, Q. “Indoor airflow and contaminant transport in a room with coupled displacement ventilation and passive-chilled-beam systems.” *Building and Environment*, 161, 106244. doi:10.1016/j.buildenv.2019.106244 (2019).

[4]. Li X, Wang X, Li X and Li Y. “Investigation on the relationship between flow pattern and air age.” *In: Sixth international IBPSA conference* (Vol. II) IBPSA, Kyoto, Japan, September 13–15 (1999).

[5]. Gholami Motlagh, V., Ahmadzadehtalatapeh, M. and Mohammadi, O. “Effect of turbulent and laminar flow mechanisms on air flow patterns and CO2 distribution in an operating room: A numerical analysis abbreviated title: Air flow pattern in an operating room*.”* *Scientia Iranica*, 30(3), pp.1008-1026 (2023).

[6]. Shetabivash, H. “Investigation of opening position and shape on the natural cross ventilation,” *Energy and Buildings*, 93, 1-15, doi.org/10.1016/j.enbuild.2014.12.053, (2015).

[7]. Qin, C., Yuanping H., Jian L., and Wei-Zhen L. "Mitigation of breathing contaminants: Exhaust location optimization for indoor space with impinging jet ventilation supply." *Journal of Building Engineering* 69 (2023): 106250.

[8]. Karava, P., Stathopoulos, T and Athienitis, A. K. “Airflow assessment in cross-ventilated buildings with operable façade elements.” *Building and Environment*, (2011), 46(1), 266–279. doi:10.1016/j.buildenv.2010.07.022.

[9]. Mohammed, R. H., “A simplified method for modeling of round and square ceiling diffusers.” *Energy and Buildings*, 64, 473–482.doi:10.1016/j.enbuild.2013.05.021 (2013).

[10]. Zhou, L and Haghighat, F., “Simplified Method for Modeling Swirl Diffusers, Department of Building,” Civil and Environmental Engineering Concordia University, Montreal, Canada, (2007).

[11]. Stamou, A. I., Katsiris, I., Schaelin, A. “Evaluation of thermal comfort in Galatsi Arena of the Olympics “Athens 2004” using a CFD model.” *Applied Thermal Engineering*, 28(10), 1206–1215. doi:10.1016/j.applthermaleng.2007.07.0 (2008).

[12]. Abid.H and Driss.Z: “Computational study and experimental validation on the effect of inlet hole surface on airflow characteristics and thermal comfort in a box occupied by thermal manikin”, *International Journal of Ventilation*, (2020) DOI: 10.1080/14733315.2020.1812223

[13]. Kobayashi, T., Sugita, K., Umemiya, N et al. “Numerical investigation and accuracy verification of indoor environment for an impinging jet ventilated room using computational fluid dynmics.“ Building *and Environment*, 115, 251– 268.doi:10.1016/j.buildenv.2017.01.022 (2017).

[14]. Chen, H. J., Moshfegh, B and Cehlin, M.,” Numerical investigation of the flow behavior of an isothermal impinging jet in a room.” *Building and Environment*, 49, 154–166.doi:10.1016/j.buildenv.2011.09.027 (2012).

[15]. Sheng .S, Yamanaka.T, Kobayashi.T et al., “Experimental study and CFD modelling of four-bed hospital ward with all-air wall induction unit for air-conditioning,” *Building and Environment*, 222, 109388, ISSN 0360-1323, https://doi.org/10.1016/j.buildenv.2022.109388.(2022)

[16]. Mohammed, R. H.,” Numerical Investigation of Displacement Ventilation Effectiveness,” *World Academy of Science, Engineering and Technology International Journal of Environmental and Ecological Engineering* Vol: 8, No:2, (2014).

[17]. Wang. J, Yin. H., Huo. H. et al., "Numerical investigation on air distribution characteristics and effect of the outlet opening mode on cross-shaped column attachment ventilation," *Building and Environment*, 233, https://doi.org/10.1016/j.buildenv.2023.110086. (2023)

[18]. Noh, K. C., Han, C.-W and Oh, M.-D. "Effect of the airflow rate of a ceiling type air-conditioner on ventilation effectiveness in a lecture room." *International Journal of Refrigeration*, 31(2), 180–188. doi:10.1016/j.ijrefrig.2007.07.005 (2008).

[19]. Rabanillo-Herrero, M., Padilla-Marcos, M. Á., Feijó-Muñoz, J. et al. "Effects of the radiant heating system location on both the airflow and ventilation efficiency in a room." *Indoor and Built Environment*, 1420326X1876528. doi:10.1177/1420326x18765282 (2018).

[20]. Tlili, O., Mhiri, H., Bournot, P., "Empirical correlation derived by CFD simulation on heat source location and ventilation flow rate in a fire room." *Energy and Buildings*, 122, 80–88. doi:10.1016/j.enbuild.2016.04.028 (2016).

[21]. Anthony, A. Sibo, Huirem Neeranjan Singh, and Tikendra Nath Verma. "Computation of turbulent natural convection in an enclosure with differential flux models." *International Journal of Heat and Mass Transfer* (2023): 123659, https://doi.org/10.1016/j.ijheatmasstransfer.2022.123659

[22]. Ganesh, G.A., Sinha, S.L., Verma, T.N. and Dewangan, S.K., "Investigation of indoor environment quality and factors affecting human comfort: A critical review," *Building and Environment*, Volume 204, 2021, 108146, ISSN 0360-1323, https://doi.org/10.1016/j.buildenv.2021.108146.

[23]. Vithanage. VN, Jayathilaka. HMKP, Jayamini. HPA., "Identification of Comfortable Zone of an Air conditioned Room with respect to the Room Dimensions and Position of A/C unit Mounted," *Conference: Sustainable Energy and Applied Engineering Technology*, (2022).

[24]. Ahmed, A. Q., Gao, S and Kareem, A. K. "A numerical study on the effects of exhaust locations on energy consumption and thermal environment in an office room served by displacement ventilation." *Energy Conversion and Management*, 117, 74–85. (2016) doi:10.1016/j.enconman.2016.03.004

[25]. Abid, H., Driss and Z., Bessrour, J. "Study of the Aerodynamic Structure in an Indoor Environment Occupied by a Human Body," *International Journal of Mechanical and Mechatronics Engineering*, Vol.19 No.03. pp. 1-18. (2019.a)

[26]. Fanger, P.O., Melikov, A.K., Hanzawa, H et al. "Air turbulence and sensation of draught." *Energy and buildings*. 1988;12:21-39

[27]. Ahmed, A.Q and Gao, S., "Numerical investigation of height impact of local exhaust combined with an office workstation on energy saving and indoor environment," *Building and Environment* (2017), doi: 10.1016/j.buildenv.2017.06.011.

[28]. Abid, H., Driss and Z., Bessrour, J. "Experimental and numerical investigation of the Reynolds number effect on indoor airflow characteristics", *Advances in Building Energy Research*, (2019.b) doi:10.1080/17512549.2019.1660711

[29]. Ganesh, G.A., Sinha, S.L., Verma, T.N. and Dewangan, S.K., "Energy consumption and thermal comfort assessment using CFD in a naturally ventilated indoor environment under different ventilations." *Thermal Science and Engineering Progress*, 50 (2024): 102557. https://doi.org/10.1016/j.tsep.2024.102557

[30]. Rajabpour, S., Hajilouy Benisi, A., T and Manzari, M. “Theoretical and experimental investigation of design parameter effects on the slip phenomenon and performance of a centrifugal compressor.” *Scientia Iranica*, *28*(1), 291-304. doi: 10.24200/sci.2020.53042.3040 (2021).

[31]. ANSYS, Inc. (2017) ANSYS FLUENT Theory Guide. Release 17.1, Canonsburg.

[32]. Abid, H., Ketata, A., Lajnef, M. et al.” Impact of greenhouse roof height on microclimate and agricultural practices: CFD and experimental investigations.” *J Therm Anal Calorim* (2024.a). https://doi.org/10.1007/s10973-024-13141-4

[33]. Norouzi, S., Hossainpour, S., and Rashidi, M. M. “Investigating the effect of train speed and ground clearance on aerodynamics of a simplified high-speed train.” *Scientia Iranica*, *30*(2), 428-441. doi: 10.24200/sci.2022.60478.6817 (2023).

[34]. Chiboub, H., Abid, H., lajnef, M, et al. “The impact of mechanical ventilation on Sfax City’s greenhouse microclimate.” *CFD Letters*, 16(8), 150–162. (2024) https://doi.org/10.37934/cfdl.16.8.150162

[35]. Jo, S., Kim, G. and Sung, M., “A study on contaminant leakage from Airborne Infection Isolation room during medical staff entry; Implementation of walking motion on hypothetical human model in CFD simulation.” *Journal of Building Engineering*, (2024) p.108812, https://doi.org/10.1016/j.jobe.2024.108812

[36]. Zhang, J., Zhao, Y., Wen, S et al.. “Assessment of COVID-19 infection Risk, thermal Comfort, and energy efficiency in negative pressure isolation wards with varied ventilation modes.” *Energy and Buildings*, p.114002. https://doi.org/10.1016/j.enbuild.2024.114002 (2024)

[37]. Foroozesh, J., Hosseini, S.H., Hosseini, A.A. et al. “CFD modeling of the building integrated with a novel design of a one-sided wind-catcher with water spray: Focus on thermal comfort.” *Sustainable Energy Technologies and Assessments*, 53, p.102736, (2022), https://doi.org/10.1016/j.seta.2022.102736

[38]. Nazemian, A., Ghadimi, P. “Automated CFD-based optimization of inverted bow shape of a trimaran ship: An applicable and efficient optimization platform.” *Scientia Iranica*, *28*(5), 2751-2768. doi: 10.24200/sci.2020.56644.4833 (2021).

[39]. Abid, H, Zghal.O, Lajnef.M et al.. "Analysis of seasonal variations and their impact on the microclimate of soilless glass greenhouses: Numerical and experimental investigations." *Numerical Heat Transfer, Part A: Applications* (2024.b): 1-25. https://doi.org/10.1080/10407782.2024.2320829

[40]. Hannachi, M, Ahmed K., Marco S., Costanza A., Tullio T., and Driss Z. "A novel pressure regulation system based on Banki hydro turbine for energy recovery under in-range and out-range discharge conditions." *Energy Conversion and Management* 243 (2021): 114417. https://doi.org/10.1016/j.enconman.2021.114417

[41]. Abid, H., Djebali, R., Faraji, H. et al. “Impact of Geometrical Parameters on Indoor Environments with Single-Sided Ventilation: Experimental and Numerical Study”, *Journal of Applied and Computational Mechanics*, (2024.c). doi: 10.22055/jacm.2024.45856.4423

[42]. Fanger, P.O and Toftum, J., “Extension of the PMV model to non-air conditioned buildings in warm climates”, *Energy and Buildings* 34 (6) (2002) 533e536.

[43]. ISO 7730, Moderate Thermal Environments e Determination of the PMV and PPD Indices and Specifications of the Conditions for Thermal Comfort, 2nd ed., International Standards Organisation, Geneva, Ref no ISO 7730:1994 (E).

Biographies

Hasna Abid is a distinguished engineer in electromechanics, holding a Ph.D. in mechanics. Her research specializes in thermal comfort and greenhouse microclimate, where she investigates airflow dynamics, energy efficiency, and sustainable practices. Dr. Abid has made significant contributions to the field, with numerous publications in prestigious international peer-reviewed journals. Her work is recognized for its depth and impact, driving advancements in both academic and practical applications of thermal management and environmental control in greenhouse settings.

Ridha Djebali is a Professor of Physics at the University of Jendouba. He holds an Engineering degree in Mechanics, a MSc in Applied Mechanics of Fluids and Heat Transfers, a PhD in Physics from the University of Tunis El Manar, and a PhD in Ceramic Materials and Surface Treatments from the University of Limoges, France. He also holds an HU degree (University Habilitation) in Physics. Prior to his academic career, Dr. Djebali worked as a process engineer in Tunisian industries specializing in general mechanics and glassmaking. He has published over 65 articles in international peer-reviewed journals and participated in more than 35 conferences in research fields including plasma jets, thin coatings, computational fluid dynamics (CFD), magnetohydrodynamics (MHD), nanofluids, heating, ventilation, and air conditioning (HVAC), boundary layers, microflow, heat exchangers, carbon-fiber-reinforced polymer composites, and optimization. He serves as a guest or permanent reviewer for over 25 journals. Currently, he leads the Research Unit Modeling, Optimization and Augmented Engineering (UR22ES12).

Hamza Faraji holds a distinguished position as a Professor at the National School of Applied Sciences, Cadi Ayyad University, located in Morocco. His expertise lies in the realm of thermal management, particularly focusing on electronic components and buildings. Prof. Dr. Faraji's research is centered around innovative approaches such as heat sinks utilizing phase change materials coupled with simple and hybrid nanoparticles, along with fins and metallic foams.

Mariem Lajnef is an engineer in electromechanics with a Ph.D. in mechanics. Her research focuses on Wind and hydro power, and she has published extensively in international peer-reviewed journals.

Zied Driss is Full Professor in the Department of Mechanical Engineering at National School of Engineers of Sfax (ENIS). He received his Engineering Diploma in 2001, his Master Degree in 2003, his PhD in 2008 and his HDR in 2013 in Mechanical Engineering from ENIS at

University of Sfax, Tunisia. He is interested on the development of numerical and experimental techniques for solving problems in mechanical engineering and energy applications.

Jamel Bessrour is Jamel Bessrour is Full Professor in the Department of Mechanical Engineering at National School of Engineers of Tunis (ENIT). He received his Engineering Diploma in 1978, his DEA Degree in 1979, his PhD in 1981 and his HDR in 2003 in Mechanical Engineering from ENIT at University of El Manar Tunisia. He is interested on the development of numerical and experimental techniques for solving problems in mechanical engineering and energy applications.

List of figures

List of tables

Table 5. Turbulence model standard deviations to experimental data at visualization line characterized by x=0.2 m and y=0.5 m

Table 6. Boundary conditions for different case studies

(a) Presentation of the cabin prototype

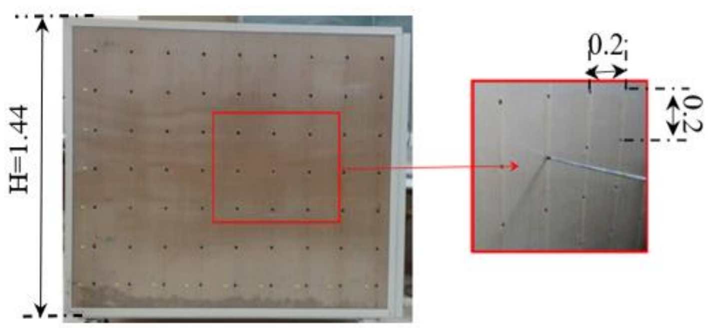

(b) Presentation of the measurement points

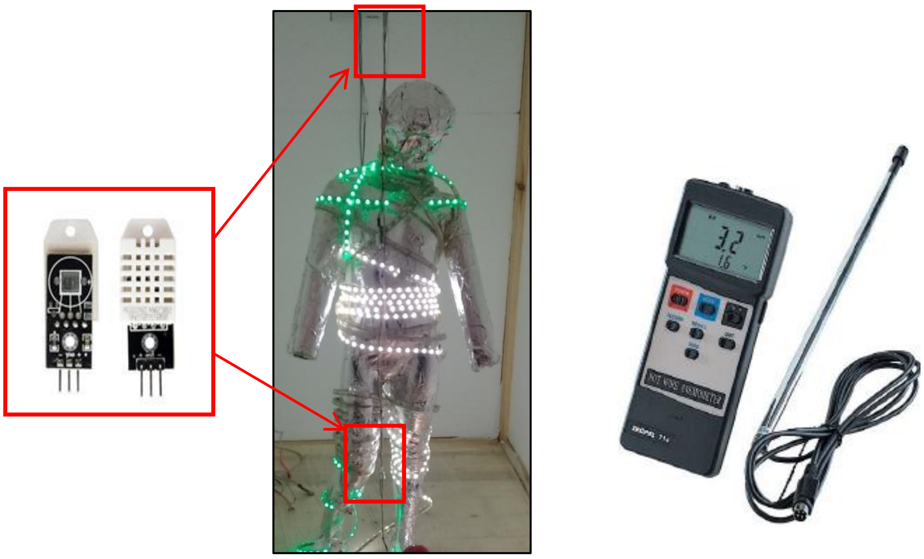

(c) thermal mannequin and air temperature sensor

(d) air velocity sensor.

Figure 2. Experimental procedure

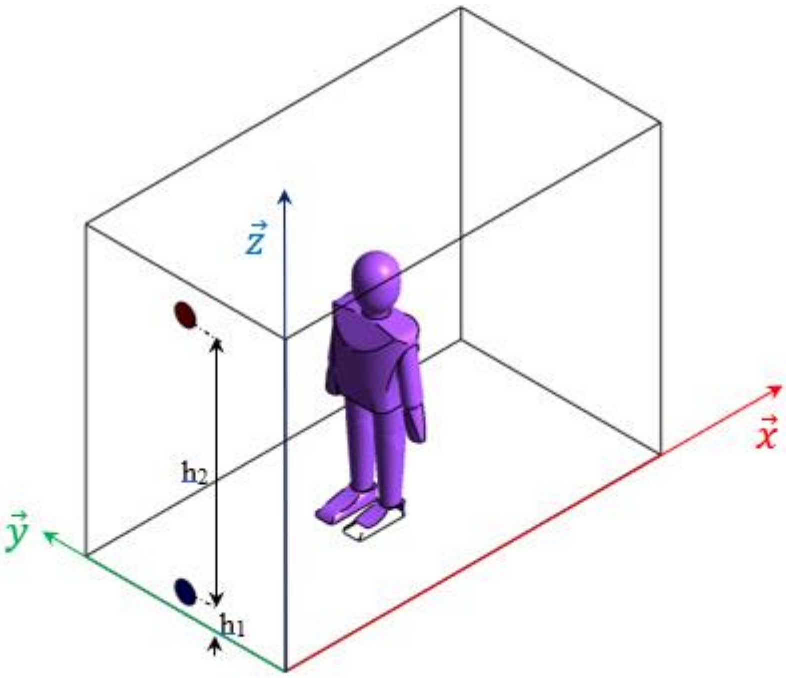

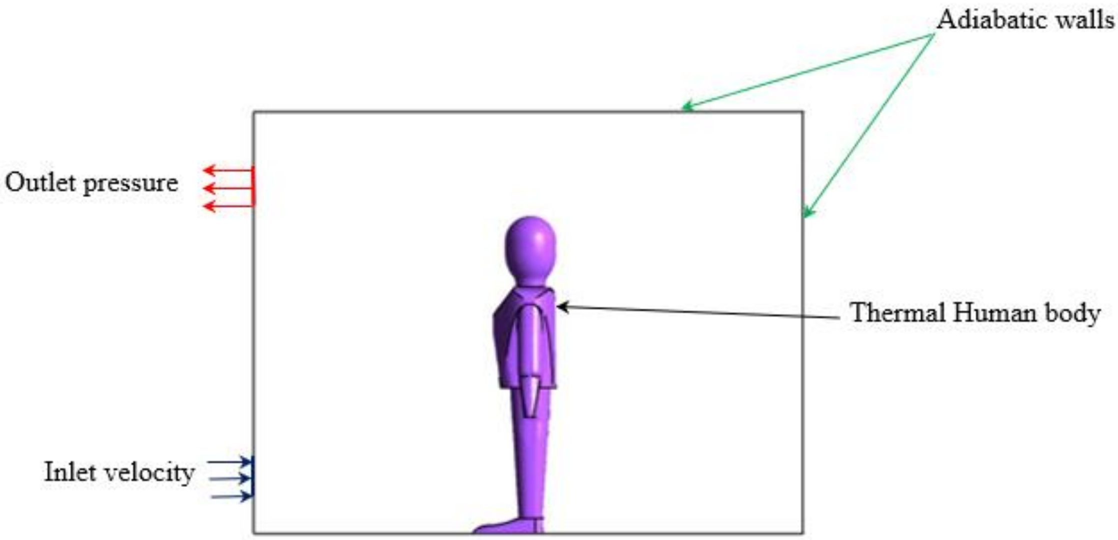

Figure 2. Computational domain and boundary conditions

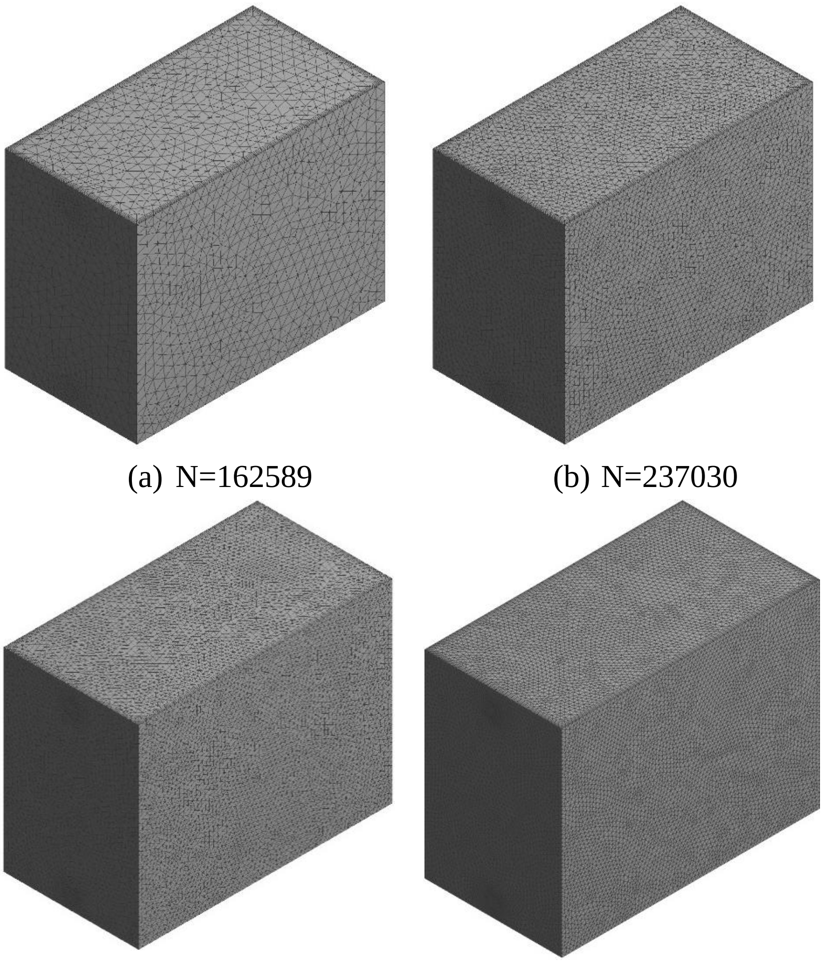

(c) N=323270 (d) N=486599

Figure 3. Different grid configurations

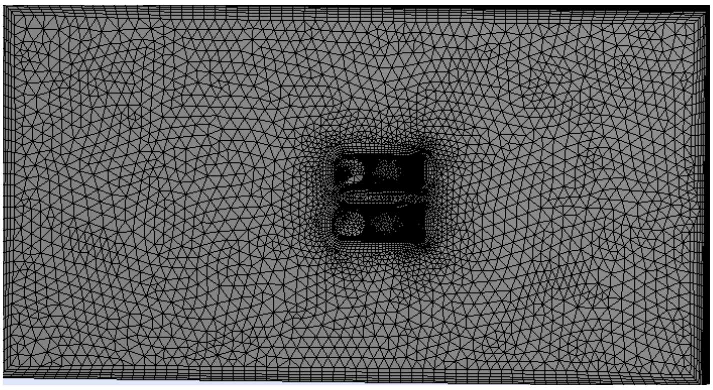

(a) Bottom view of the mesh

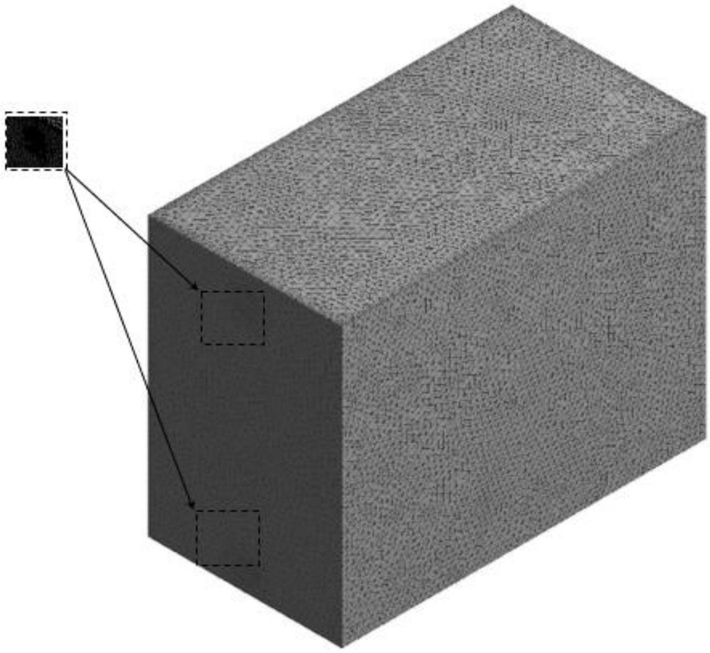

(b) Computational domain meshing.

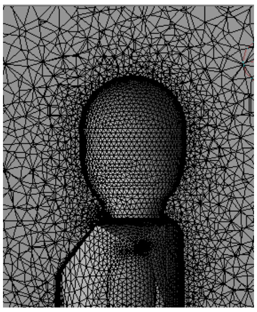

(c) Visualization of the mesh around the human body

Figure 4. Presentation of the considered meshing

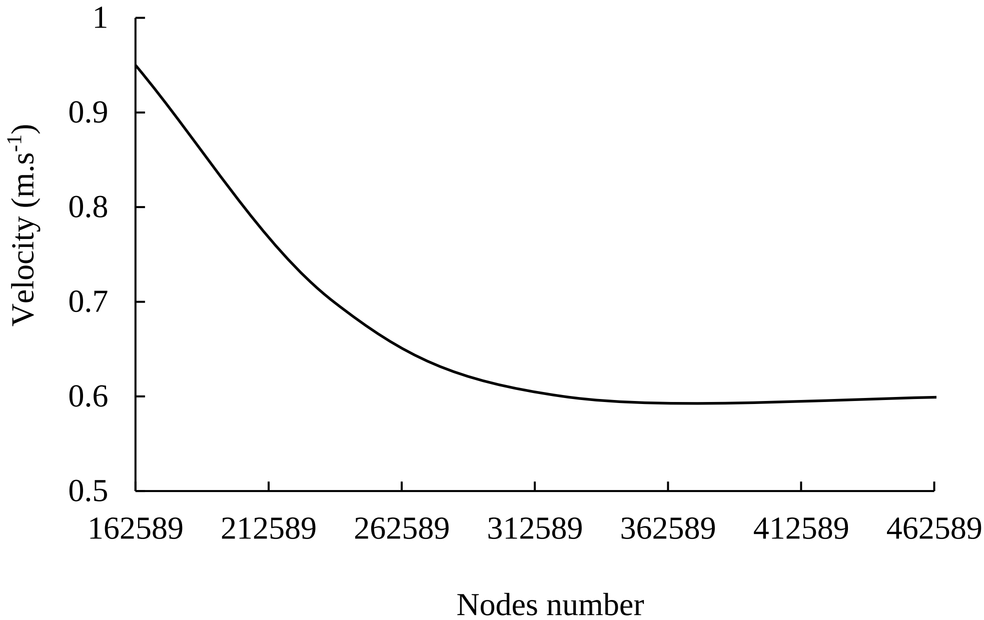

Figure 5. Mesh selection: Velocity value for various meshes at the position described by x=0.74 m, y=0.5 m, and z=0.05 m

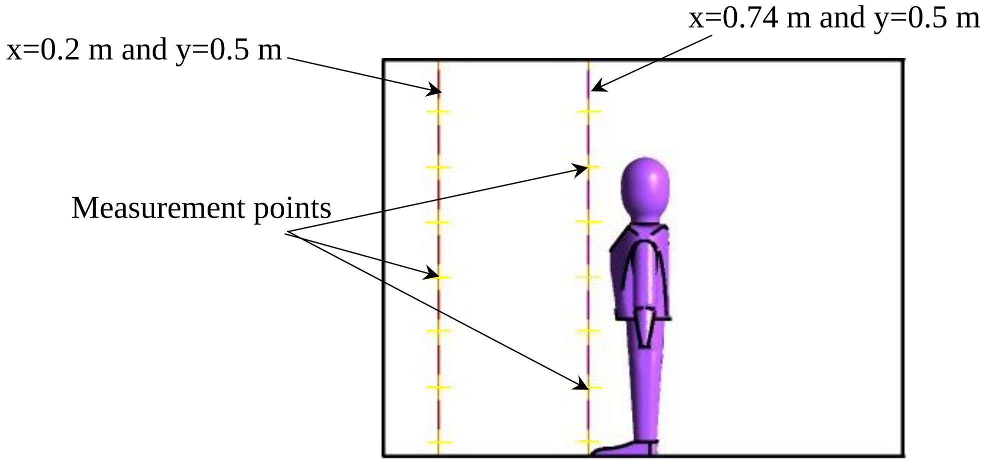

(a) Visualization of the directions specified by (x=0.2 m, y=0.5 m) and (x=0.74 m, y=0.5 m) and the measurement points.

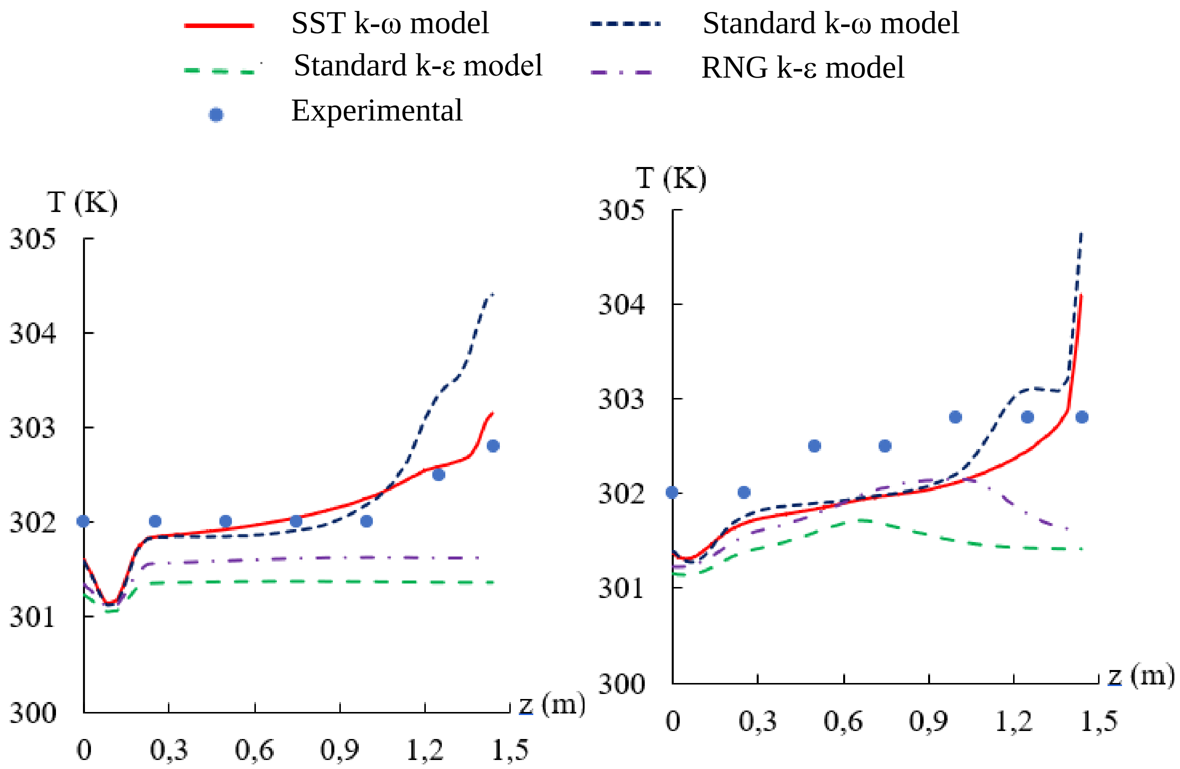

(b) Temperature profile long x = 0.2 m and y=0.5 m

(c) Temperature profile long x =0.74 m and y=0.5 m

Figure 6. Turbulence model effect on temperature profiles

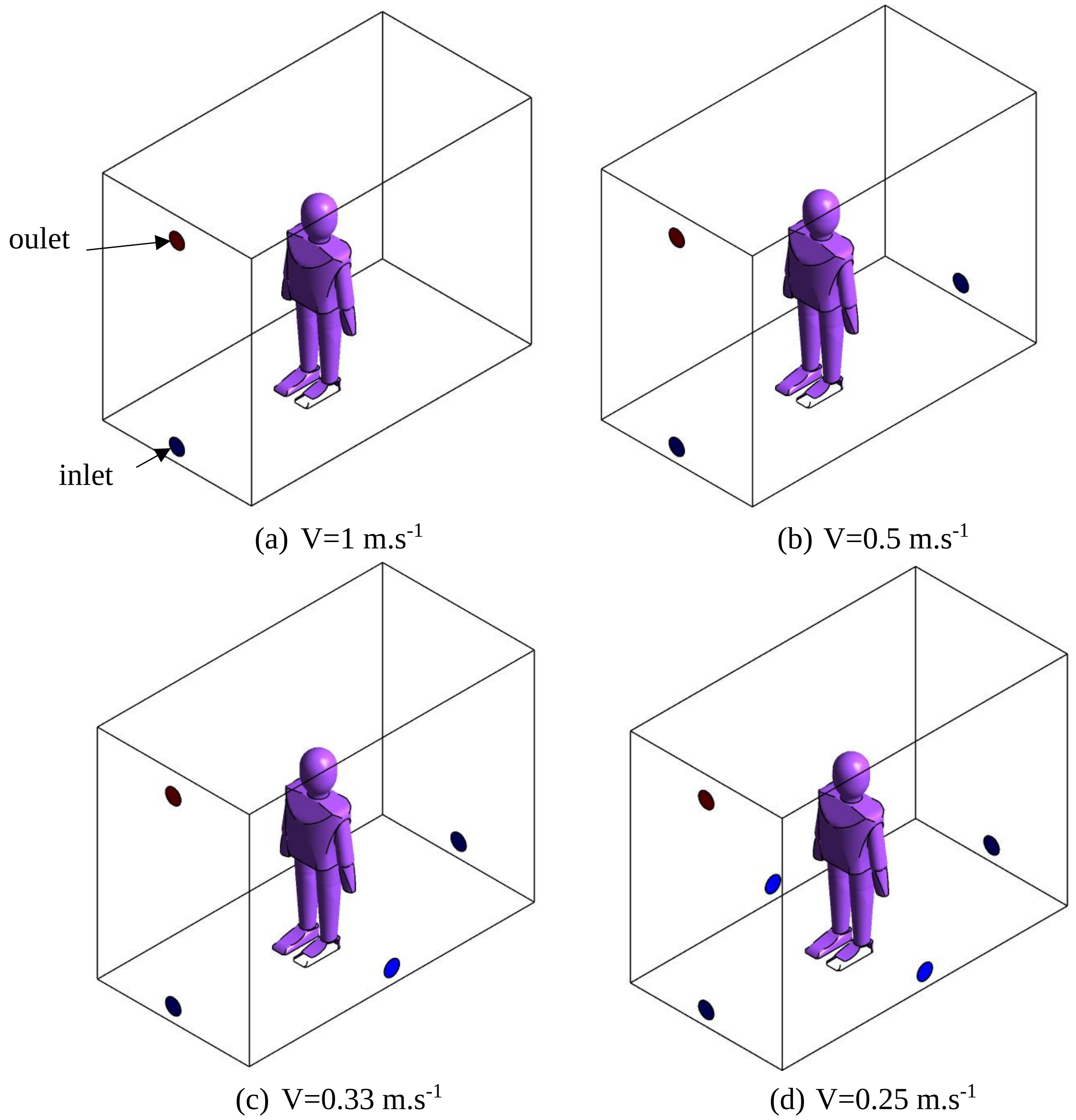

Figure 7. The different computational domain

V=1 m.s^{-1} V=0.5 m.s^{-1} V=0.33 m.s^{-1}
V=0.25 m.s^{-1} Experimental

V (m.s^{-1}) V (m.s^{-1})

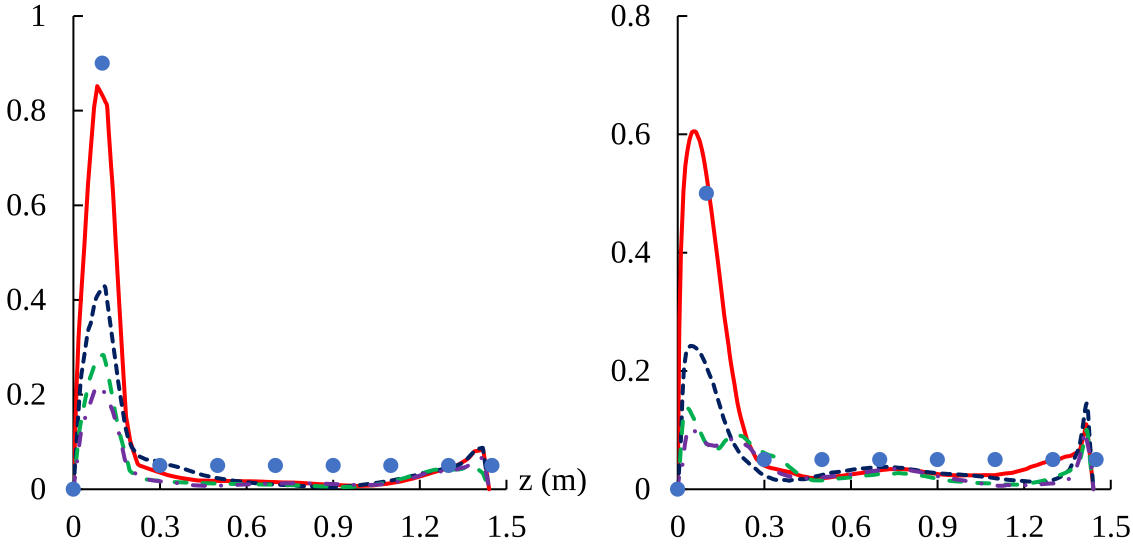

(a) x=0.2 m (b) x=0.72 m

Figure 8. Velocity profiles in the plane defined by y=0.5 m.

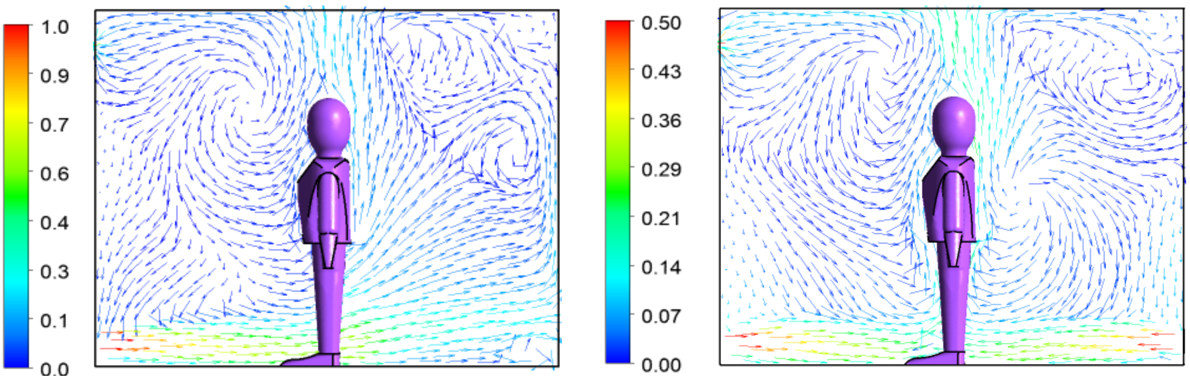

(a) V=1 m.s^{-1} (b) V=0.5 m.s^{-1}

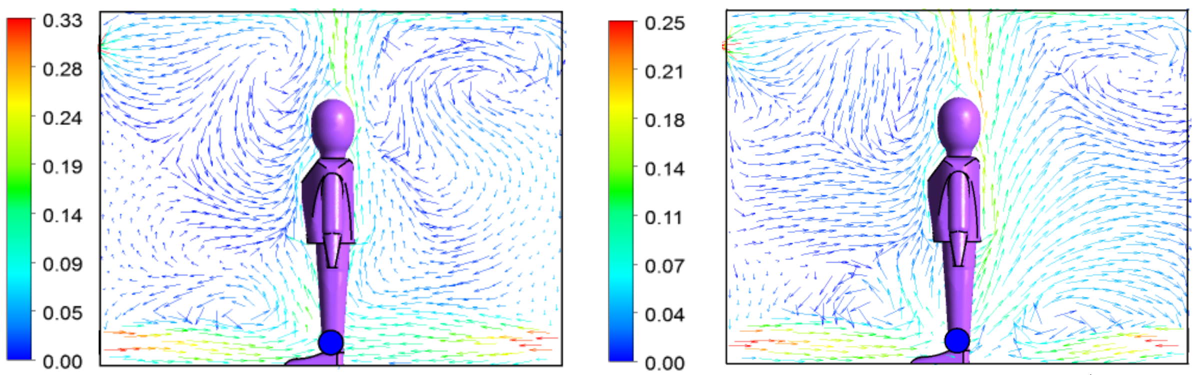

(c) V=0.33 m.s^{-1} (d) V=0.25 m.s^{-1}

Figure 9. Simulated velocity fields distribution (m.s^{-1}) in the middle cross section of room (y=0.5m).

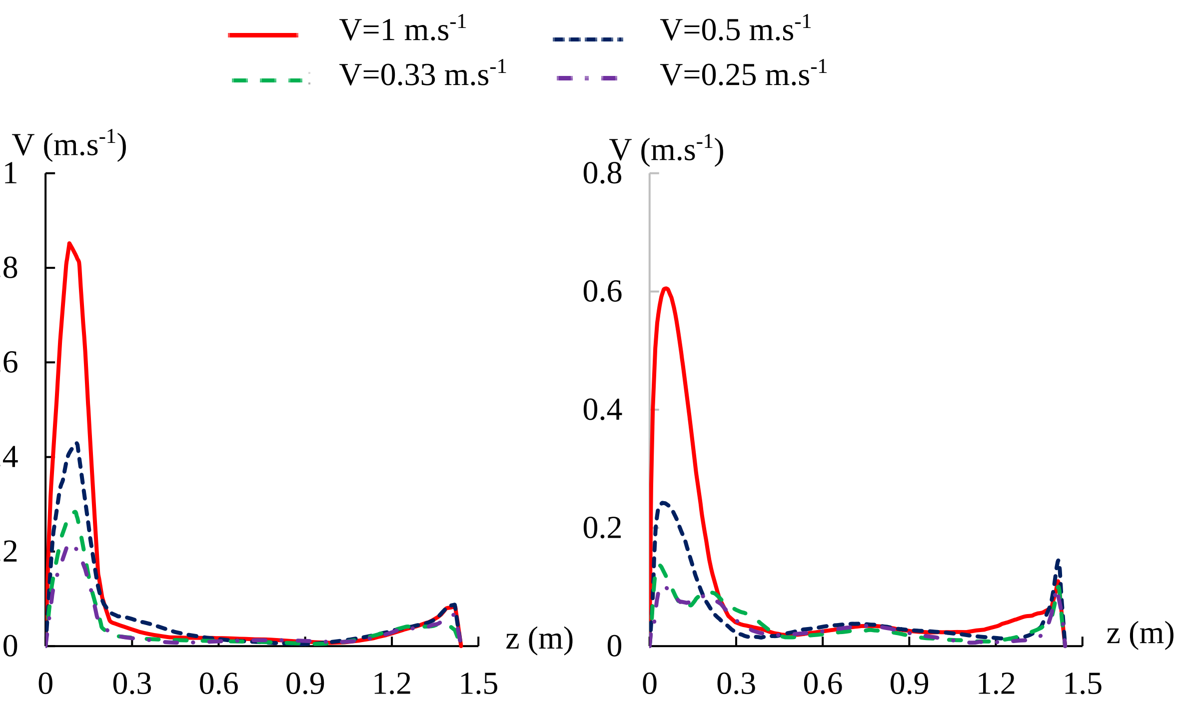

(a) x = 0.2 m (b) x = 0.74 m

Figure 10. Velocity profiles in the direction defined by (x=0.2m, y = 0.5 m) and (x=0.74m, y = 0.5 m)

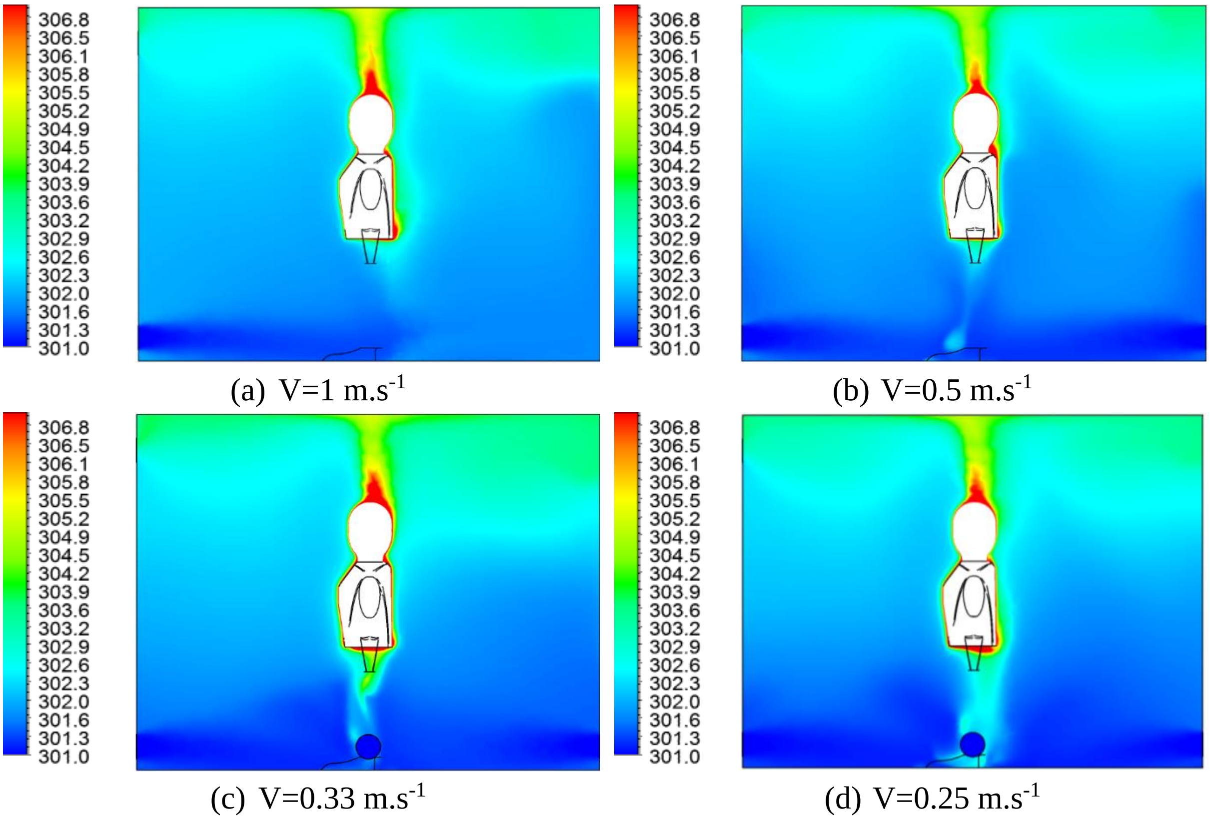

(a) V=1 m.s^{-1} (b) V=0.5 m.s^{-1}

(c) V=0.33 m.s^{-1} (d) V=0.25 m.s^{-1}

Figure 11. Simulated temperature distribution (K) in the middle cross section of room (y=0.5 m).

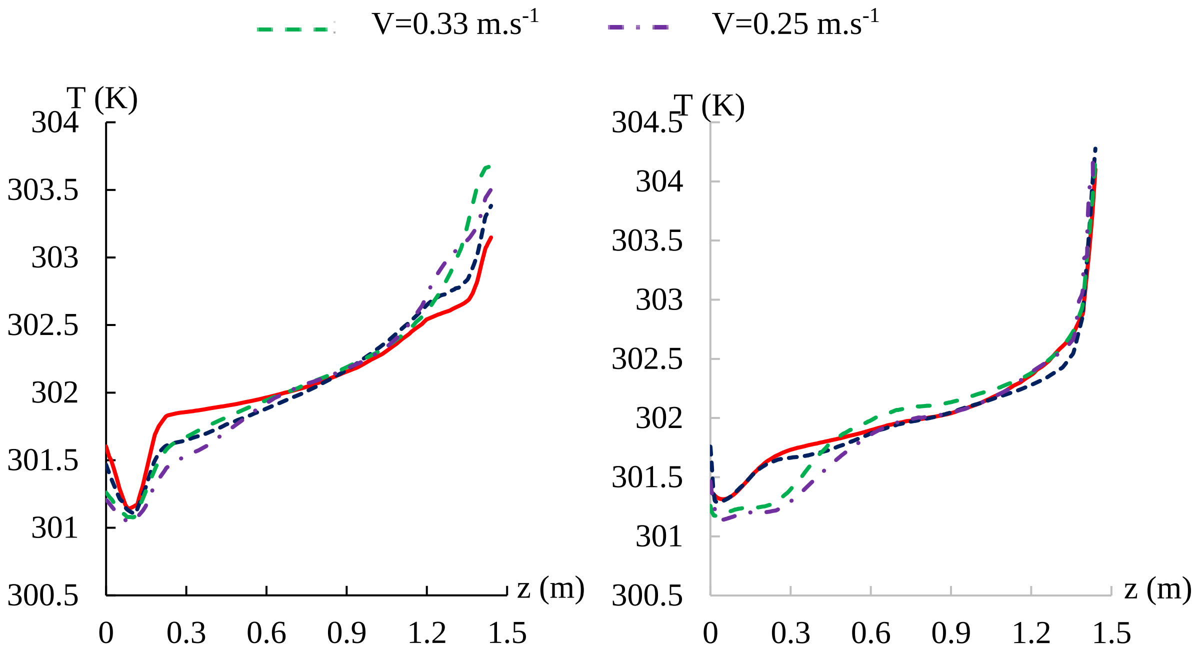

(a) x=0.2 m and y=0.5 m (b) x=0.74 m and y=0.5 m

Figure 12. Profile temperature in Z direction

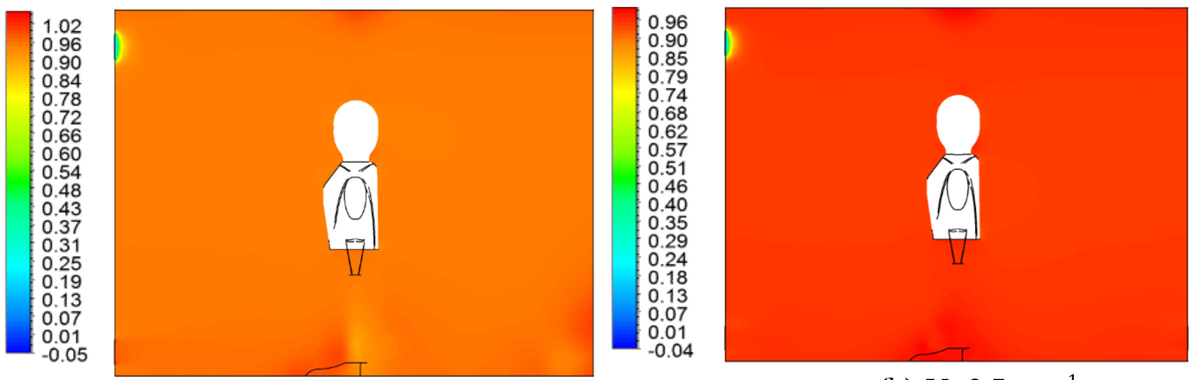

(a) V=1 m.s^{-1} (b) V=0.5 m.s^{-1}

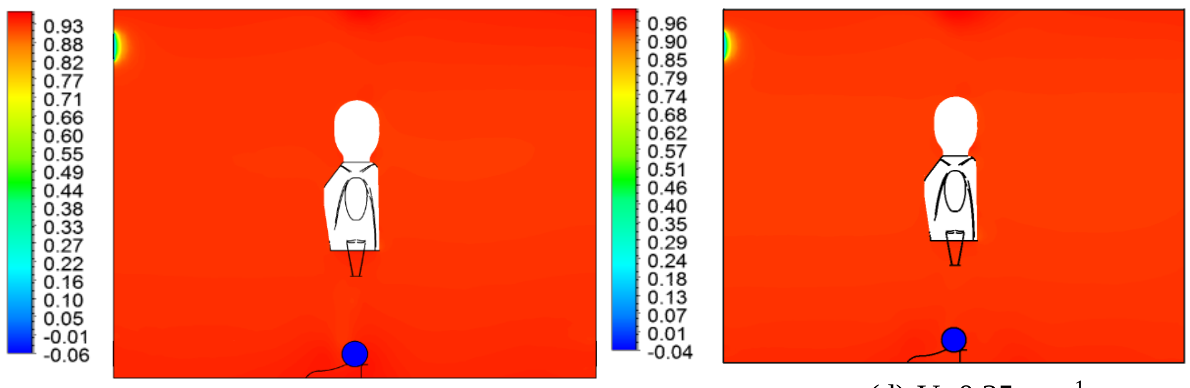

(c) V=0.33 m.s^{-1} (d) V=0.25 m.s^{-1}

Figure 13. Simulated static pressure distribution (Pa) in the middle cross section of room (y=0.5m).

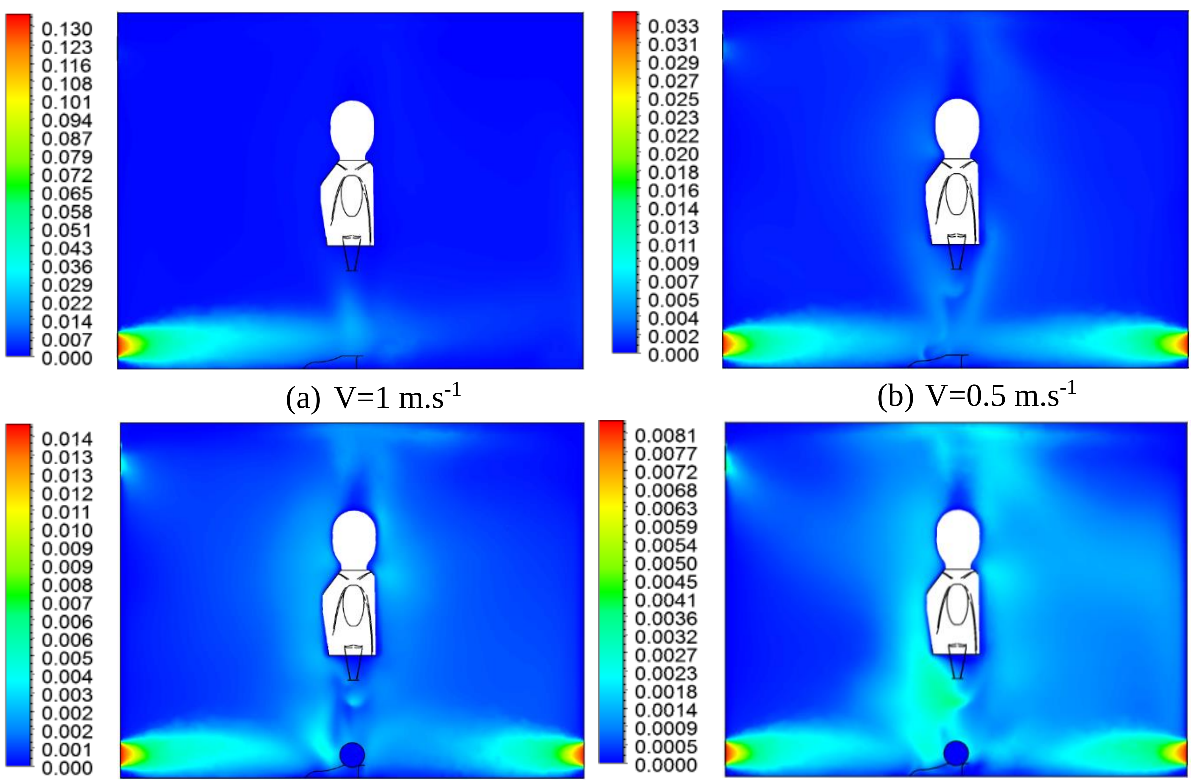

(a) V=1 m.s^{-1} (b) V=0.5 m.s^{-1}

(c) V=0.33 m.s^{-1} (d) V=0.25 m.s^{-1}

Figure 14. Simulated turbulent kinetic energy distribution ($m^2.s^{-2}$) in the middle cross section of room (y=0.5m).

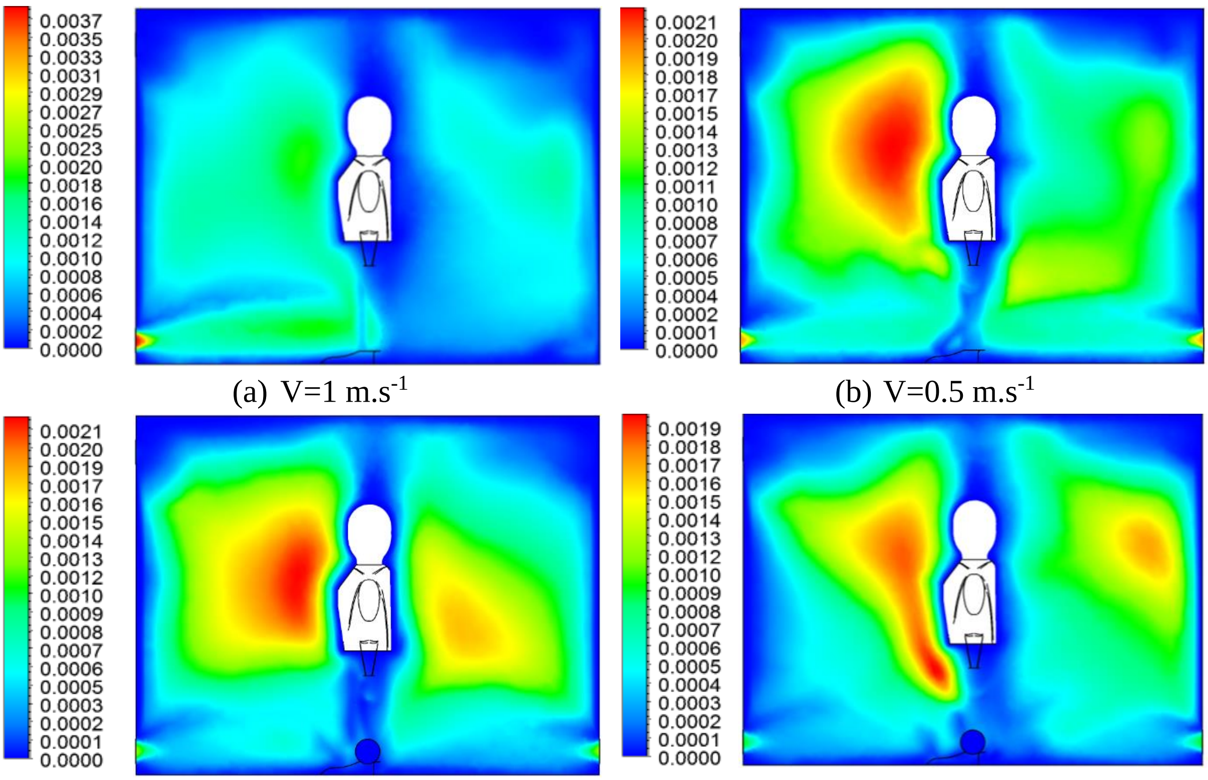

(a) V=1 $m.s^{-1}$ (b) V=0.5 $m.s^{-1}$

(c) V=0.33 $m.s^{-1}$ (d) V=0.25 $m.s^{-1}$

Figure 15. Simulated turbulent viscosity distribution ($kg.m^{-1}.s^{-1}$) in the middle cross section of room (y=0.5m).

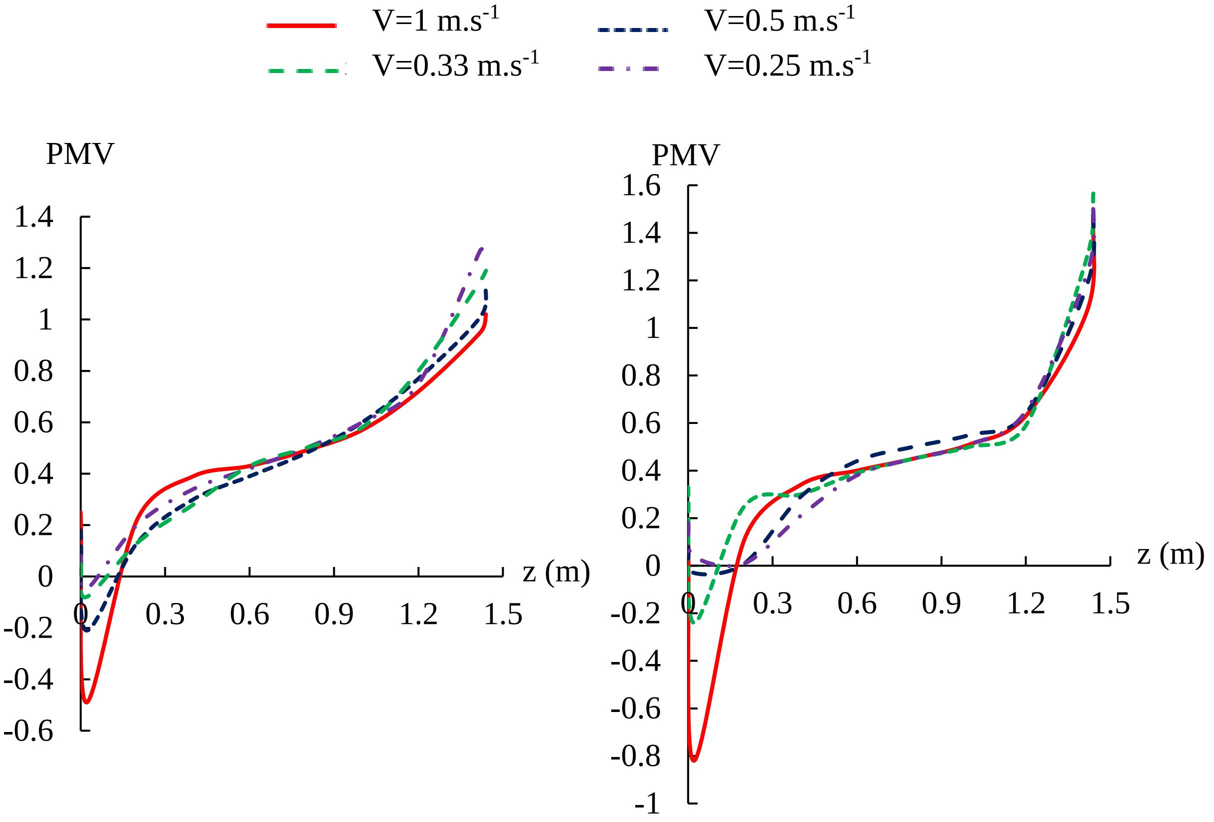

(a) x=0.2 m and y=0.5 m (b) x=0.72 m and y=0.5 m

Figure 16. PMV profiles in Z direction

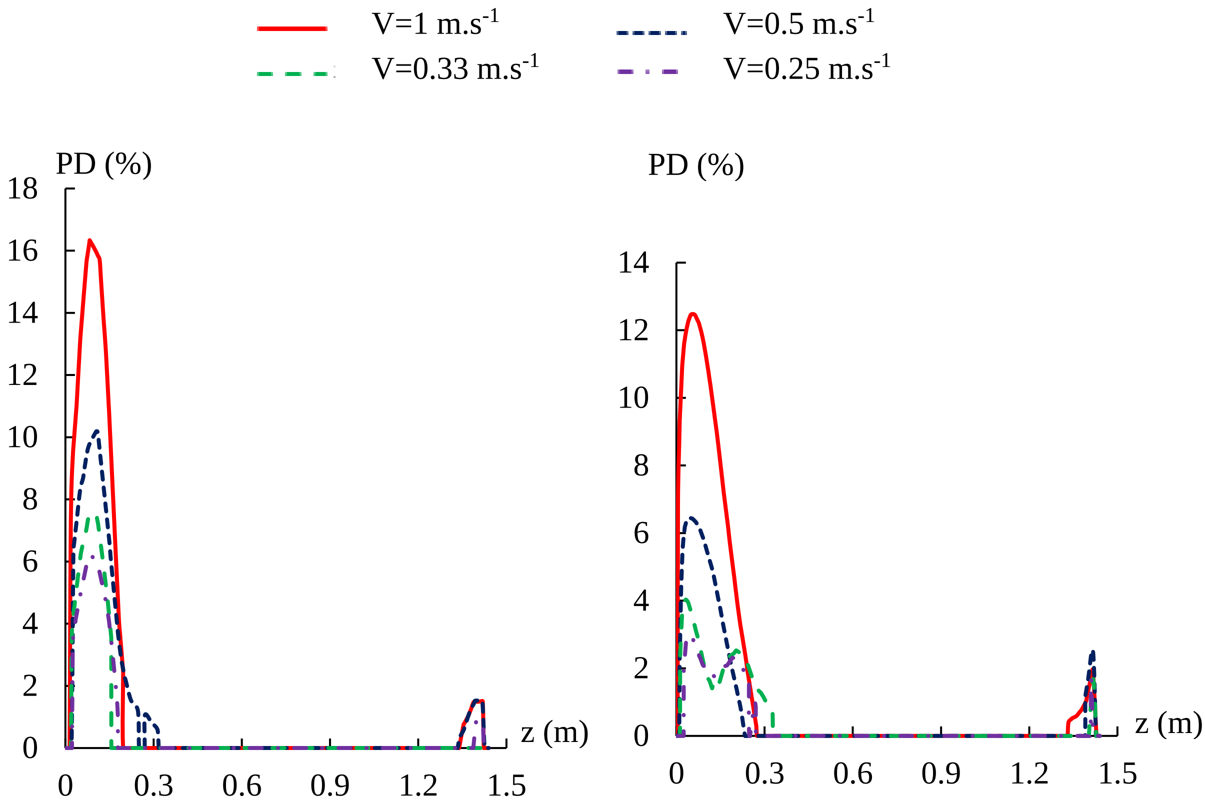

(a) x =0.2 m and y=0.5 m (b) x =0.72 m and y=0.5 m

Figure 17. PD (%) profiles for different inlet velocity in Z direction

Table 1. Test cabin design parameters.

Design parameters	Value
Test cabin length, $L(m)$	1.88
Test cabin width, $W(m)$	1
Test cabin height, $H(m)$	1.45
Distance between the ground and the inlet opening, $h_1(m)$	0.095

Distance between the inlet opening and the outlet opening, $h_2(m)$	1.2
Opening dimension, $D(m)$	0.1
Thermal Human body height, $h_o(m)$	1

Table 2 The Hot-wire anemometer type AM 4204 characteristics.

Description	**Hot wire anemometer type AM4204**
Manufacturer	Lutron
Probe type	Telescopic
Measurement parameters	Air velocity+ Temperature+ Gaz flow

Resolution	Air velocity 0.1 m. s^{-1} Temperature 0.1°C
Precision	Air velocity 5% Temperature ±0.8°C
Measuring range	Air velocity from 0.2-20 m. s^{-1} Temperature -20°C to +70°C

Table 3. Presentation of the boundary conditions

Surface	Type	Value
Cabin Inlet	Velocity inlet	V=1 m.s^{-1}
Cabin Inlet	Inlet temperature	T=301 K
Cabin Inlet	Inlet turbulence intensity	Tu=5%
Cabin outlet	Pressure outlet	P= zero-gauge pressure
Cabin walls/ roof	Opaque wall	q=0 W.m^{-2}
Thermal Human body	Heat flux	Q=45 W.m^{-2}

Table 4. Meshing characteristics

Case	Node number	Cell number
M1	162589	516641
M2	237030	734981
M3	323270	1093754
M4	586599	1731086

Table 5. Turbulence model standard deviations to experimental data at visualization line characterized by x=0.2 m and y=0.5 m

z (m)	SST k-ω model	Standard k-ω model	RNG k-ε model	Standard k-ε model
0	0,16556291	0,23178808	0,29801325	0,23178808
0.3	0,06622517	0,16556291	0,26490066	0,16556291
0.5	0	0,16556291	0,26490066	0,16556291
0.8	0	0,16556291	0,26490066	0,16556291
1	0,06622517	0,16556291	0,26490066	0,16556291
1.3	0,03305785	0,33057851	0,42975207	0,33057851
1.5	0,0660502	0,42932629	0,52840159	0,42932629

Table 6. Boundary conditions for different case studies

Case	Inlet velocity ($m.s^{-1}$)	Inlet opening number	Inlet temperature (K)
1	1	1	301
2	0.5	2	301
3	0.3	3	301
4	0.25	4	301